Open Archive TOULOUSE Archive Ouverte (OATAO)

OATAO is an open access repository that collects the work of Toulouse researchers and makes it freely available over the web where possible.

Estimating the Intrinsic Dimension of Hyperspectral Images Using a Noise-Whitened Eigengap Approach

Abderrahim Halimi, *Member, IEEE*, Paul Honeine, *Member, IEEE*, Malika Kharouf,
Cédric Richard, *Senior Member, IEEE*, and Jean-Yves Tourneret, *Senior Member, IEEE*

Abstract—**Linear mixture models are commonly used to represent a hyperspectral data cube as linear combinations of endmember spectra. However, determining the number of endmembers for images embedded in noise is a crucial task. This paper proposes a fully automatic approach for estimating the number of endmembers in hyperspectral images. The estimation is based on recent results of random matrix theory related to the so-called spiked population model. More precisely, we study the gap between successive eigenvalues of the sample covariance matrix constructed from high-dimensional noisy samples. The resulting estimation strategy is fully automatic and robust to correlated noise owing to the consideration of a noise-whitening step. This strategy is validated on both synthetic and real images. The experimental results are very promising and show the accuracy of this algorithm with respect to state-of-the-art algorithms.**

Index Terms—**Eigengap approach, endmember number, hyperspectral imaging, linear spectral mixture, random matrix theory (RMT), sample covariance matrix.**

I. INTRODUCTION

UNMIXING techniques can provide fundamental information when analyzing multispectral or hyperspectral images with limited spatial resolution. In spite of almost 50 years of research in this area, there has been a surge of interest in the last few years within the area of remote sensing and hyperspectral imaging [1], [2]. Even with an ever-increasing spatial resolution, each pixel (or spectrum) in a hyperspectral image is generally associated with several pure materials. Each spectrum can thus be seen as a mixture of spectral signatures called endmembers with respective proportions called abundances. While nonlinear unmixing techniques have been recently investigated [3]–[5], the linear mixing model is widely accepted because of its natural physical interpretation. This model assumes that each spectrum is a convex combination of the endmember spectra. Unmixing hyperspectral images consists of three stages: 1) determining the number of endmembers and possibly projecting the data onto a subspace of reduced dimension [6], [7]; 2) extracting endmember spectra [8], [9]; and 3) estimating their abundances [10]–[12]. These stages can be performed separately or jointly [13]–[15]. Determining the number of endmembers, or the signal subspace dimension, then appears as a fundamental step in order to achieve endmember spectrum determination and abundance estimation. This paper considers this problem of estimating the signal subspace dimension of hyperspectral images.

Estimating the number of endmembers present in a scene has been described under several names and under different methodological frameworks. The most well-known definitions are based on the eigenvalues of the sample (observation) covariance matrix, with the so-called "virtual dimension" (VD) as well as many variants, including the "intrinsic dimension" and the "effective dimension." The VD is estimated by the so-called Harsanyi–Farrand–Chang (HFC) method which relies on the Neyman–Pearson detection theory applied to the difference between the eigenvalues of the sample covariance matrix and its noncentered counterpart (i.e., the matrix of second-order moments) [7]. The HFC and its noise-whitened version (NWHFC) are generally more efficient than algorithms based on model selection criteria such as the Akaike information criterion (AIC) [16] and the minimum description length (MDL) [17], [18], particularly in the presence of colored noise. The idea of evaluating the differences between the eigenvalues of the covariance and the correlation matrices has also been exploited in other algorithms such as [19]. In [6], the authors proposed a fully automatic approach for hyperspectral subspace identification called Hysime. Their method consists of minimizing a cost function whose aim is to reduce the noise power. Other methods only use the sample covariance matrix without considering the correlation matrix. In [7], the noise subspace projection method considers a Neyman–Pearson test to separate noise components from signal components based on a whitened covariance

matrix. The idea is that the noise eigenvalues are equal to unity while the signal eigenvalues are greater than one.

Random matrix theory (RMT) is a universal multivariate statistics tool that has been used successfully in many fields. Recently, an approach based on RMT has been applied to estimate the number of endmembers [20]. This method (denoted by NWRMT) first estimates the noise covariance matrix in order to remove colored noise effects. Then, based on the whitened covariance eigenvalues, this method proposes a theoretical threshold to determine the number of endmembers in the image. However, this method appears to be sensitive to noise [20], [21] which might reduce the estimation performance. Moreover, it has been shown in [22] that many noise estimation algorithms are sensitive to noise correlation. In the presence of such correlations, the NWRMT algorithm [20] may provide results of poor quality.

The motivation of this paper is to provide a consistent and fully automatic estimator of the number of endmembers by considering a general scenario, where the additive noise components are not identically distributed. The main advantage of the proposed approach, with respect to (w.r.t.) the NWRMT algorithm, is its robustness in the presence of correlated noise. Similarly to the NWRMT and Hysime approaches, our method starts by estimating the noise covariance matrix in order to remove its effect from the sample/observation covariance matrix. The next step is inspired from recent results on spiked population models (SPMs) [23]. Indeed, the authors of [24] proposed a method based on the gap between successive eigenvalues of the sample covariance matrix. By considering sorted eigenvalues, the main idea is that the gap between eigenvalues (of a whitened covariance) is larger in the presence of a signal while it is reduced for noise components. Building on this idea, an automatic threshold is obtained to separate the signal from noise components.

Contributions and Comparisons: The main objective of this paper is to provide a fully automatic algorithm for estimating the number of endmembers in hyperspectral images. The proposed approach generalizes the consistent estimator proposed in [24] for independent and identically distributed (i.i.d.) noise to the colored Gaussian noise case. This eigengap approach is based on a consistent estimator, while the NWRMT algorithm [20] is not fully consistent as stated in [24]. The proposed approach appears to be more robust to correlated noise and to small image sizes. These statements are validated on both synthetic and real hyperspectral images.

This paper is organized as follows. Section II introduces the hyperspectral mixing model, the SPM, and the rank estimation methods for an SPM. Section III introduces our algorithm whose performance is evaluated in Section IV on synthetic images. Results on real hyperspectral images are presented in Section V. Conclusion and perspectives for future works are finally reported in Section VI.

II. PROBLEM FORMULATION

A. LMM

The linear mixture model (LMM) assumes that each pixel spectrum $\boldsymbol{y}_n$, of size $L \times 1$, is a linear combination of K endmembers $\boldsymbol{m}_k$, $k \in \{1, \ldots, K\}$, corrupted by an additive noise $\boldsymbol{e}_n$ as follows:

$$\boldsymbol{y}_n = \sum_{k=1}^{K} a_{kn} \boldsymbol{m}_k + \boldsymbol{e}_n$$
$$= \boldsymbol{M} \boldsymbol{a}_n + \boldsymbol{e}_n \tag{1}$$

where $\boldsymbol{e}_n \sim \mathcal{N}(\boldsymbol{0}_L, \boldsymbol{\Sigma})$ is a Gaussian noise, $\boldsymbol{\Sigma}$ is the noise covariance matrix, $\boldsymbol{0}_L$ is an $L \times 1$ vector of 0, $\boldsymbol{a}_n = [a_{1n}, \ldots, a_{Kn}]^\top$ is the $K \times 1$ abundance vector of the nth pixel, and $\boldsymbol{M} = [\boldsymbol{m}_1, \ldots, \boldsymbol{m}_K]$ is an $L \times K$ matrix gathering the endmember spectra. The abundance vector $\boldsymbol{a}_n$ contains proportions satisfying the positivity and sum-to-one (PSTO) constraints $a_{kn} \geq 0$, $\forall k \in \{1, \ldots, K\}$ and $\sum_{k=1}^{K} a_{kn} = 1$. Considering N pixels gathered in the $L \times N$ matrix $\boldsymbol{Y}$, the LMM can be written as follows:

$$\boldsymbol{Y} = \boldsymbol{M} \boldsymbol{A} + \boldsymbol{E} \tag{2}$$

where $\boldsymbol{A}$ is a $K \times N$ matrix of abundances and $\boldsymbol{E}$ is an $L \times N$ matrix of noise samples.

Rank estimation can be based on an eigenvalue analysis of the covariance matrix of $\boldsymbol{Y}$. Assuming independence between the signal counterpart $\boldsymbol{S} = \boldsymbol{M} \boldsymbol{A}$ and the noise $\boldsymbol{E}$ leads to

$$\boldsymbol{R}_Y = \boldsymbol{R}_S + \boldsymbol{\Sigma} \tag{3}$$

where $\boldsymbol{R}_Y$ and $\boldsymbol{R}_S$ are the covariance matrices of $\boldsymbol{Y}$ and $\boldsymbol{S}$, respectively. In this paper, we are interested in estimating the number K of endmembers, which is equal to $R + 1$, where $R = \text{rank}(\boldsymbol{R}_S)$. Indeed, the signal lies into a subspace of dimension $K - 1$ because of the PSTO constraints.

B. SPM

A well-known model in RMT is the SPM. This model assumes that the covariance matrix of interest has all its eigenvalues equal to σ^2 except a few eigenvalues (known as spikes) as follows [23], [24]:

$$\boldsymbol{\Lambda} = \sigma^2 \boldsymbol{\Gamma} \begin{bmatrix} \gamma_1 & & & \\ & \ddots & & \boldsymbol{0}_{R,L-R} \\ & & \gamma_R & \\ \hline & \boldsymbol{0}_{L-R,R} & & \boldsymbol{I}_{L-R} \end{bmatrix} \boldsymbol{\Gamma}^\top \tag{4}$$

where $\boldsymbol{\Lambda}$ is the covariance matrix, $\boldsymbol{\Gamma}$ is an $L \times L$ orthogonal matrix, $\boldsymbol{0}_{i,j}$ is the $i \times j$ matrix of 0, and $\boldsymbol{I}_L$ is the $L \times L$ identity matrix. Determining the number of endmembers can be performed by computing the number of spiked eigenvalues of the covariance matrix $\boldsymbol{\Lambda}$. For this purpose, consider that $\boldsymbol{R}_Y = \boldsymbol{\Lambda}$, and denote its eigenvalues by λ_r for $r = 1, \ldots, L$. By assuming[1] $\boldsymbol{\Sigma} = \sigma^2 \boldsymbol{I}_L$ and the eigenvalue vector $[\rho_1, \ldots, \rho_R, \boldsymbol{0}_{1,L-R}]^\top$ for $\boldsymbol{R}_S$, (3) leads to

$$\rho_r + \sigma^2 = \gamma_r \sigma^2, \text{ for } r \leq R \tag{5}$$

---

[1]In the presence of colored noise, an adequate procedure will be considered as shown in the following.

and (4) yields

$$\lambda_r = \begin{cases} \rho_r + \sigma^2, & \text{if } r \le R \\ \sigma^2, & \text{otherwise.} \end{cases} \qquad (6)$$

Unfortunately, in many situations, the covariance matrix $\boldsymbol{R}_S$ is unknown, and the additive noise is not necessarily identically distributed, contradicting the assumption $\boldsymbol{\Sigma} = \sigma^2 \boldsymbol{I}_L$. The alternative proposed in this paper builds an estimator of the number of endmembers when only the sample covariance matrix $\boldsymbol{R}_Y$ is known and $\boldsymbol{e}_n$ is an additive independently and not identically distributed zero-mean Gaussian noise sequence.

C. Rank Estimation From an SPM

Estimating the number of spikes from an SPM is an interesting problem that has found many applications, including chemical mixtures [25] and hyperspectral unmixing [20]. A recent work proposed to investigate RMT to estimate the number of spikes or endmembers in hyperspectral images [20]. This work builds on the estimator proposed in [25] in the context of chemical mixtures. This method uses the following assumptions: (i) $N \to \infty$ and $L \to \infty$ (or large values of N and L) with $c = (L/N) > 0$ a positive constant; (ii) the noise corrupting the data is Gaussian and independent of the signal; and (iii) the signal covariance matrix has a fixed rank R. Under these assumptions, the method [20], [25] is based on the study of the asymptotic behavior of the largest eigenvalues of the sample covariance matrix when both the dimension of the observations and the sample size grow to infinity at the same rate. The main idea is that, when the covariance matrix $\boldsymbol{\Lambda}$ is a perturbed version of a finite rank matrix, all but a finite number of eigenvalues of the covariance matrix are different from the i.i.d. noise variance. Based on this property and on [23] and [26], a threshold that separates the eigenvalues corresponding to the useful information from those corresponding to the noise was derived in [20] and [25], yielding

$$\widehat{R} = \min_{r=1,\dots,L} \left(\lambda_r < \sigma^2 \left(\frac{\beta_c}{N^{\frac{2}{3}}} s(\alpha) + (1 + \sqrt{c})^2 \right) \right) - 1 \quad (7)$$

where $\lambda_1 \ge \lambda_2 \ge \cdots \ge \lambda_L$ are the eigenvalues of the sample covariance matrix $\boldsymbol{\Lambda}$, $s(\alpha)$ can be found by using the Tracy–Widom distribution, and

$$\beta_c = (1 + \sqrt{c})(1 + \sqrt{c^{-1}})^{\frac{1}{3}}. \qquad (8)$$

This estimator is based on a sequence of nested hypothesis tests. By construction, the proposed estimator is not fully consistent as shown in [27]. In this paper, we are interested in deriving a new estimator with better statistical properties.

One of the front-line research problems in RMT is the study of the gap between consecutive eigenvalues [24], [26], [27]. Indeed, the eigenvalue differences can be used for the estimation of the number of spikes under the following assumptions [24], [28]: (i) N and L are related by the asymptotic regime

$N \to \infty$, $(L/N) \to c > 0$; (ii) the noise corrupting the data is assumed Gaussian and independent of the signal;[2] (iii) the signal covariance matrix has a fixed rank R; (iv) the eigenvalues of the sample covariance matrix are of multiplicity one;[3] and (v) $\gamma_1 > \cdots > \gamma_R > 1 + \sqrt{c}$ which is referred to as the separation condition. Note first that, under hypotheses (i) and (v), it is shown in [26] that the eigenvalues of the covariance matrices of SPMs satisfy almost surely

$$\lambda_r \xrightarrow[N \to \infty]{a.s.} \sigma^2 \phi(\gamma_r) \qquad (9)$$

for each $r \in \{1, \dots, R\}$, while for $r > R$

$$\lambda_r \xrightarrow[N \to \infty]{a.s.} \sigma^2 (1 + \sqrt{c})^2 \qquad (10)$$

where $\phi(x)$ is defined by

$$\phi(x) = (x + 1) \left(1 + \frac{c}{x} \right). \qquad (11)$$

These results were used in [24] and [29] to infer the number of components R in the case where $\sigma^2 = 1$. In the general case where $\sigma^2 \ne 1$, the authors of [24] stated that one should divide the eigenvalues by the noise variance σ^2 to apply the results obtained for $\sigma^2 = 1$. The estimation method in [24] considers the following differences between successive eigenvalues:

$$\delta_r = \lambda_r - \lambda_{r+1}, \text{ for } r = 1, \dots, L - 1. \qquad (12)$$

The main idea is that, when approaching nonspiked values, the eigengap δ_r shrinks to small values. Therefore, the number of endmembers can be estimated as follows:

$$\widehat{R} = \min \left\{ r \in \{1, \dots, M\}; \delta_{r+1} < d_N \right\} \qquad (13)$$

where $M \ge R$ is a fixed integer (large enough) and $d_N \xrightarrow{N \to \infty} 0$ is a threshold to determine. According to [24], the consistency of this estimator is ensured if $d_N \to 0$ and $N^{2/3} d_N \to +\infty$. The same authors proposed to use $d_N = (\psi_N/N^{2/3})\beta_c$ with $\psi_N = 4\sqrt{2 \log(\log N)}$ that satisfies the former conditions. The obtained algorithm was fully automatic in the sense that it did not require tuning any parameter. The main difference between this strategy and that in [20] and [25] is that the one in [24] builds a test statistics based on the gaps between successive eigenvalues and not on the eigenvalues themselves. An important consequence is that a theoretical estimator consistency is ensured in the case of the gap approach while the method described in [20] and [25] depends on a parameter α and is nearly consistent as stated in [24].

---

[2]This assumption is introduced to satisfy [24, Assumption 3.1]. However, the Gaussianity of the additive noise is not necessary, and the proposed approach is valid under less restrictive assumptions described in the Appendix.

[3]This assumption is also considered in NWHFC and HFC algorithms [7], [19] as well as in the ELM algorithm [19]. The general case of eigenvalues with multiple multiplicities has been considered in [27] and will be studied in future works.

III. Proposed Algorithm

The eigengap strategy assumes the noise to be i.i.d., which is not true when considering hyperspectral images [6], [30]. Therefore, we propose to use a preliminary step before estimating the number of endmembers.

A. Noise Estimation

A great effort has been devoted to the noise estimation problem since it is essential for many signal processing applications requiring whitening and/or dimension reduction. Among these algorithms, we distinguish those assuming spatial homogeneous regions such as the nearest neighbor difference (NND) [31], the geometrical based algorithm [32], and algorithms estimating the noise such as the multiple regression-based methods [6], [7], [33]. The NND algorithm requires homogenous areas that are not always available in hyperspectral images [6]. The Meer algorithm does not account for noise spectral correlation since it estimates the noise variance for each band separately [34]. This paper considers the multiple regression-based method proposed in [6] since it has been studied in many subspace identification algorithms [34], [35] and has shown similar results as the residual method in [7] as stated in [34]. However, the proposed approach is still valid when considering other noise estimation algorithms.

The multiple regression method [6] assumes that the ℓth spectral band of each pixel vector is connected to the other $L-1$ bands by a linear model. More precisely, denoting by $\boldsymbol{y}_\ell$ the $N \times 1$ vector containing the pixel elements of the ℓth band and by $\boldsymbol{Y}_{-\ell}$ the $(L-1) \times N$ matrix obtained by removing the ℓth row from the matrix $\boldsymbol{Y}$, we assume that

$$\boldsymbol{y}_\ell = \boldsymbol{Y}_{-\ell}^\top \boldsymbol{b}_\ell + \boldsymbol{\epsilon}_\ell \tag{14}$$

where $\boldsymbol{\epsilon}_\ell$ is the modeling error vector of size $N \times 1$ and $\boldsymbol{b}_\ell$ is the $(L-1) \times 1$ regression vector that is estimated using the least squares estimator [6]

$$\widehat{\boldsymbol{b}}_\ell = \left(\boldsymbol{Y}_{-\ell}\boldsymbol{Y}_{-\ell}^\top\right)^{-1} \boldsymbol{Y}_{-\ell}\boldsymbol{y}_\ell. \tag{15}$$

The noise vector is then estimated by $\widehat{\boldsymbol{\epsilon}}_\ell = \boldsymbol{y}_\ell - \boldsymbol{Y}_{-\ell}^\top \widehat{\boldsymbol{b}}_\ell$, and its covariance matrix is given by

$$\widehat{\boldsymbol{\Sigma}} = \frac{(\widehat{\boldsymbol{\epsilon}}_1, \ldots, \widehat{\boldsymbol{\epsilon}}_L)^\top (\widehat{\boldsymbol{\epsilon}}_1, \ldots, \widehat{\boldsymbol{\epsilon}}_L)}{N}. \tag{16}$$

Once the noise covariance matrix has been estimated, a whitening procedure can be performed as described in the next section.

B. Rank Estimation

Before applying the eigengap test, let us first remove the effect of colored noise. This can be achieved by whitening the observed pixels $\boldsymbol{Y}$ using the estimated noise covariance matrix $\widehat{\boldsymbol{\Sigma}}$. However, it has been shown in [20] and [21] that this procedure leads to an overestimated subspace dimension R when combined to RMT approaches. Therefore, we will consider the strategy used in [20] which is valid even in the case of a full noise covariance matrix. Under the assumption that $\boldsymbol{v}_i^\top \boldsymbol{w}_i \neq 0, \forall i = 1, \ldots, L$, it has been shown in [20] that

$$\widehat{\lambda}_r = \begin{cases} \rho_r + \frac{\boldsymbol{v}_r^\top \widehat{\boldsymbol{\Sigma}} \boldsymbol{w}_r}{\boldsymbol{v}_r^\top \boldsymbol{w}_r}, & \text{if } r \leq R \\ \frac{\boldsymbol{v}_r^\top \widehat{\boldsymbol{\Sigma}} \boldsymbol{w}_r}{\boldsymbol{v}_r^\top \boldsymbol{w}_r}, & \text{otherwise} \end{cases} \tag{17}$$

where $\boldsymbol{v}_r$ and $\boldsymbol{w}_r$ denote the eigenvectors of $\boldsymbol{R}_Y$ and $\boldsymbol{R}_S$, respectively. Note that (17) is similar to (6) except that the noise term has been estimated differently as

$$\widehat{\sigma}_r^2 = \frac{\boldsymbol{v}_r^\top \widehat{\boldsymbol{\Sigma}} \boldsymbol{w}_r}{\boldsymbol{v}_r^\top \boldsymbol{w}_r}. \tag{18}$$

Note that (18) converts the effect of the full matrix $\widehat{\boldsymbol{\Sigma}}$ to an equivalent independent noise (whose variance is $\widehat{\sigma}_r^2$) which makes the proposed estimator more robust (see the next section). Equations (17) and (18) require the computation of the eigenvectors of $\boldsymbol{R}_S$. The covariance matrix $\boldsymbol{R}_S$ is unknown but can be estimated using (3) as follows:

$$\widehat{\boldsymbol{R}}_S = \boldsymbol{R}_Y - \widehat{\boldsymbol{\Sigma}}. \tag{19}$$

Finally, to account for colored noise, one has to include the noise variance (18) in (9) and (10) by dividing each eigenvalue λ_r by the corresponding noise variance $\widehat{\sigma}_r^2$, as stated in [24]. The resulting rank estimator is given by

$$\widehat{R} = \min \{r \in \{1, \ldots, M\}; \Delta_{r+1} < d_N\} \tag{20}$$

with

$$\Delta_r = \frac{\widehat{\lambda}_r}{\widehat{\sigma}_r^2} - \frac{\widehat{\lambda}_{r+1}}{\widehat{\sigma}_{r+1}^2} \text{ and } d_N = \frac{\psi_N}{N^{\frac{2}{3}}}\beta_c. \tag{21}$$

The resulting algorithm is summarized in Algorithm 1.

Algorithm 1 Proposed NWEGA Algorithm

1: Compute the sample covariance matrix $\boldsymbol{R}_Y$
2: Estimate the noise covariance matrix $\widehat{\boldsymbol{\Sigma}}$
3: Compute the matrix $\boldsymbol{V}$ containing the eigenvectors of $\boldsymbol{R}_Y$ (sorted in descending order of the eigenvalues)
4: Compute the matrix $\boldsymbol{W}$ containing the eigenvectors of $\widehat{\boldsymbol{R}}_S = \boldsymbol{R}_Y - \widehat{\boldsymbol{\Sigma}}$ (sorted in descending order of the eigenvalues)
5: Compute $\widehat{\lambda_r}$, $r \in \{1, \ldots, L\}$, the eigenvalues of $\boldsymbol{R}_Y$ (sorted in descending order)
6: Compute $\widehat{\sigma_r^2}$ according to (18)
7: Compute Δ_r and d_N according to (21)
8: Estimate the number of endmembers $\widehat{K} = \widehat{R} + 1$ by evaluating (20)

IV. Simulation Results on Synthetic Data

This section analyzes the performance of the proposed noise-whitened eigengap approach (NWEGA) with simulated data. The proposed approach is first compared to EGA (considering $\sigma^2 = 1$ in all bands) to highlight the benefit of the noise-whitening step. NWEGA is also compared to the NWHFC

approach since it has been shown in [7] to provide better results than the approaches based on information criteria such as AIC [16] and MDL [17], [18]. Note that the NWHFC algorithm[4] requires the definition of the false alarm probability P_f. We have considered in our experiments three values $P_f \in \{10^{-3}, 10^{-4}, 10^{-5}\}$ denoted by NWHFC$_1$, NWHFC$_2$, and NWHFC$_3$, respectively. The NWEGA is also compared to the NWRMT approach proposed in [20] since it uses similar theoretical tools. Indeed, this method uses a noise-whitening step as described in Section III-A followed by the estimator presented in (7). The well-known Hysime algorithm [6] is also investigated since it has been used in many studies [20], [35]. The considered data sets were constructed based on the USGS spectra library used in [6]. As in [20], we considered 20 minerals that vary widely (some spectra are similar, others are different, some spectra have low amplitude, etc.). These spectra are shown in [36] but are not represented here for brevity. The abundances were drawn uniformly in the simplex defined by the PSTO constraints using a Dirichlet distribution [6]. The following sections present three kinds of results: (i) robustness w.r.t. noise; (ii) impact of the image size; and (iii) performance w.r.t. the number of endmembers. In all these experiments, we considered the parameters $N = 10^4$ pixels, $L = 224$ bands, SNR $= 25$ dB, and $K = 4$ endmembers when fixed according to the experimental setup (i), (ii), or (iii). We performed 50 Monte Carlo simulations for each experiment.

A. Robustness to Noise

This section studies the robustness of the proposed approach w.r.t. noise. Two experiments were considered. The first experiment studies the performance of the different algorithms when the noise variance is inaccurately estimated. Except EGA that assumes $\sigma^2 = 1$ for all spectral bands, the studied algorithms account for a noise estimation step that may introduce some errors. Therefore, we simulated synthetic images using $K = 4$ fixed endmembers (chosen from the 20 spectra) with an i.i.d. Gaussian noise with variance σ^2 (corresponding to SNR $=$ 25 dB). Then, we applied the noise-whitened algorithms when considering a noise variance given by $\sigma^2(1 + \epsilon)$, to simulate an error in the noise estimation step. Fig. 1 shows the obtained accuracy (in percent) of the estimated number of endmembers when varying ϵ (the accuracy represents the percentage of good estimates). This figure shows the failure of EGA in capturing the number of endmembers, highlighting the need for the noise-whitening step (the noise level and shape affects the EGA performance). It also shows the robustness of the remaining algorithms w.r.t. noise overestimation. However, observe that both NWRMT and Hysime algorithms are sensitive to noise variance underestimation since they provide incorrect results for $\epsilon \leq -0.1$ and $\epsilon \leq -0.4$, respectively. The results show the robustness of the proposed NWEGA since it provides an accuracy higher than 90% for $\epsilon > -0.5$. The best performance was
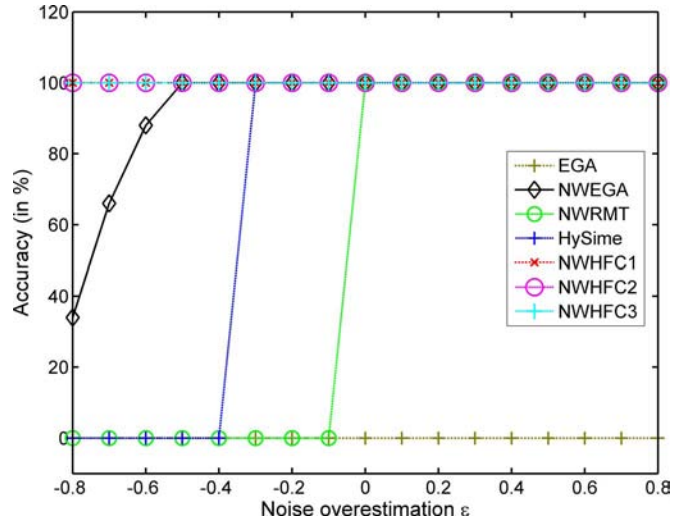

Fig. 1. Robustness of the algorithms w.r.t. the accuracy of the noise estimation.

obtained with the NWHFC approach. This algorithm applies a Neyman–Pearson test on the difference between covariance and correlation eigenvalues. Therefore, the additive noise perturbation introduced by $(1 + \epsilon)$ is eliminated (or greatly reduced). The proposed NWEGA is more robust than NWRMT and Hysime to noise estimation errors, which is of great interest, particularly when considering real data.

The second experiment considers the effect of the noise correlation between the different spectral bands denoted as spectral correlation, which is generally observed in real data [22], [34]. To simulate data with spectral correlation, we considered the following covariance structure[5] when band j is correlated with band $j + 1$ with a correlation coefficient C:

$$\mathbf{\Sigma} = \begin{bmatrix} \sigma_1^2 & 0 & & \cdots & & 0 \\ 0 & \ddots & & & & \vdots \\ \vdots & & \sigma_j^2 & C\sigma_{j+1}^2 & & \\ & & C\sigma_{j+1}^2 & \sigma_{j+1}^2 & & \\ & & & & \ddots & \\ 0 & 0 & \cdots & & & \sigma_L^2 \end{bmatrix}. \quad (22)$$

This covariance structure was chosen to compare our results with that in [34], which used a similar matrix structure. We first varied the number of correlated spectral bands when considering a correlation coefficient $C = 0.5$. The correlated bands are chosen randomly from the set $\{1, \ldots, L-1\}$. For all the algorithms, we considered the noise estimation algorithm described in Section III-A. Fig. 2 (top) shows a linear evolution of $\widehat{K}$ w.r.t. the number of correlated bands for both NWRMT and Hysime (which is in agreement with the results in [34]). Both NWEGA and NWHFC show a stable result as the number of correlated bands increases. Note that NWEGA presents the best results. In a second study, we varied C when considering ten correlated bands (drawn randomly between 1 and L). The

---

[4]The NWHFC is obtained by preceding the HFC algorithm by a noise-whitening step. We have considered the HFC algorithm available in: http://www.ehu.es/computationalintelligence/index.php/Endmember_Induction_Algorithms.

[5]We represented the covariance structure for one correlated band j. The case of multiple correlated bands can be obtained by considering multiple values for j.
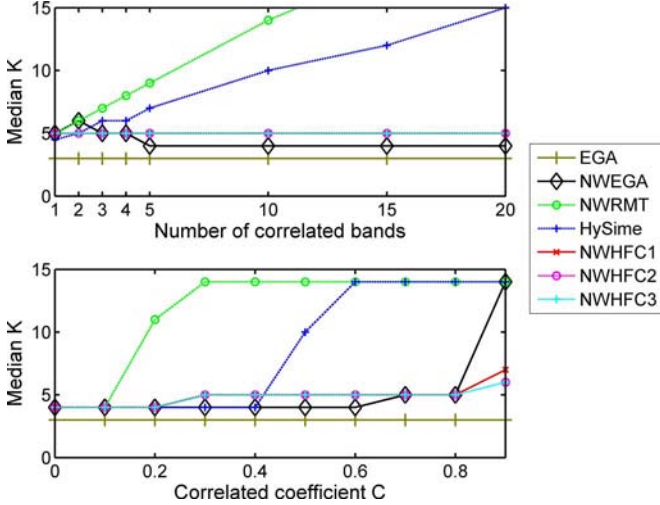
Fig. 2. Estimated K w.r.t. (top) number of correlated bands and (bottom) variation of the correlation coefficient. The actual number of endmembers is $K = 4$.

TABLE I
ESTIMATED K WITH RESPECT TO THE IMAGE SIZE N. ESTIMATED
MEDIAN VALUE AND THE ACCURACY IN PERCENT BETWEEN BRACKETS

Method	$N = 10^2$	$N = 20^2$	$N = 30^2$	$N = 50^2$	$N = 10^4$
EGA	2 (0)	2 (0)	3 (0)	3 (0)	3 (0)
NWEGA	100 (0)	4 (86)	4 (100)	4 (100)	4 (100)
NWRMT	100 (0)	63 (0)	23 (0)	8 (0)	4 (100)
HySime	100 (0)	98 (0)	29 (0)	4 (100)	4 (100)
NWHFC$_1$	67 (0)	4 (100)	4 (100)	4 (100)	4 (100)
NWHFC$_2$	66 (0)	4 (100)	4 (100)	4 (100)	4 (100)
NWHFC$_3$	66 (0)	4 (100)	4 (100)	4 (100)	4 (100)

results are shown in Fig. 2 (bottom). The NWEGA shows the best performance except for $C > 0.8$ where NWHFC has more stable results. To summarize, the obtained results highlight the need for the noise-whitening step and illustrate the robustness of the NWEGA w.r.t. noise estimation error and noise correlation. It is more robust to noise correlation than NWRMT, Hysime, and NWHFC. Both NWEGA and NWHFC are robust to noise estimation error.

B. Robustness to the Image Size

As described in Section II-C, EGA and NWEGA are valid when $\gamma_1 > \cdots > \gamma_R > 1 + \sqrt{c}$, with $c = L/N$. While this condition suggests that the image size should be large to obtain good results, we will see in this section that acceptable results are also obtained for small images. The simulated images were obtained by using the previous $K = 4$ endmembers and an i.i.d. Gaussian noise with SNR = 25 dB. Table I shows the median of the estimated $\widehat{K}$ over 50 Monte Carlo results, and the obtained accuracy indicated between brackets when varying the image size. Without a noise-whitening step, EGA fails in capturing the endmember number for all image sizes. All the remaining algorithms provided poor results for $N = 100$. However, both NWEGA and NWHFC provided accurate estimates for $N \geq 400$ pixels. Hysime offered accurate estimates for $N \geq 2500$ pixels, while NWRMT required the largest number of pixels, $N = 10000$ pixels. These results show that the asymptotic

regime of NWEGA is reached for smaller values of N than for the NWRMT approach. Indeed, the NWEGA is based on a consistent estimator, while the NWRMT algorithm is not fully consistent as recently demonstrated in [24]. Note that the obtained results are also in agreement with those in Section IV-A. Indeed, the estimated noise covariance $\widehat{\Sigma}$ in (16) depends on the considered number of pixels, i.e., a reduced number of pixels increases the estimation error of $\widehat{\Sigma}$. Therefore, algorithms that are robust to noise estimates are expected to perform better when reducing the image size, which is observed in Table I. To conclude, the results of this section show the fast convergence of NWEGA w.r.t. N, which makes this algorithm applicable even for small images.

C. Performance

This section studies the performance of the NWEGA when varying the number of endmembers, the noise level, and the noise shape, as in [6] and [35]. The synthetic images were generated using the standard parameters described in Section IV. For each Monte-Carlo simulation, the endmembers were randomly chosen in a database containing 20 minerals. Moreover, and similarly to [6] and [35], we considered two noise shapes w.r.t. spectral bands: 1) a constant shape w.r.t. spectral bands which represents an i.i.d. Gaussian noise and 2) a Gaussian shape for the noise variance w.r.t. spectral bands defined as follows:

$$\sigma_\ell^2 = \sigma^2 \frac{\exp\left[\frac{-(\ell - L/2)^2}{(2\eta^2)}\right]}{\sum_i^L \exp\left[\frac{-(i - L/2)^2}{(2\eta^2)}\right]}, \ \ell = 1, \ldots, L \quad (23)$$

where σ^2 is fixed according to the required SNR and η controls the width of the Gaussian shape of the noise variance. Table II shows the obtained results with an i.i.d. Gaussian noise.[6] This table shows that all the algorithms provide good estimates for all SNRs when considering a reduced number of endmembers $K \leq 5$. However, the NWHFC algorithm shows poor results for large values of K even for high SNRs. Note that the Hysime, NWRMT, and NWEGA algorithms provide good estimates for high SNR (SNR > 25 dB) while the Hysime performance decreases for low SNR. Note finally that NWRMT and NWEGA provide similar performance. Table III shows the results when considering a Gaussian shape for the noise variance. This table shows poor results for NWHFC even for small values of K. However, the results are slightly improved when using the actual noise covariance matrix instead of the estimated one (see results between brackets). The Hysime, NWRMT, and NWEGA algorithms have a similar behavior as shown in Table II, i.e., the Hysime performance decreases for low SNR while the NWRMT and NWEGA results are slightly better. These results show the accuracy of the NWEGA that provides equal or better results than the state-of-the-art algorithms.

---

[6]Without a noise-whitening step, EGA estimated 3 endmembers for all scenarios.

TABLE II
MEDIAN OF THE ESTIMATED K FOR DATA CORRUPTED BY
WHITE NOISE (50 MONTE CARLO SIMULATIONS). FOR NWHFC,
WE SHOW BETWEEN BRACKETS THE RESULTS WHEN USING
THE GROUND-TRUTH NOISE COVARIANCE MATRIX

SNR	Method	K=3	K = 5	K = 10	K = 15
15 dB	NWEGA	**3**	**5**	7	**8**
	NWRMT	3	5	**8**	8
	HySime	3	4	5	4
	NWHFC$_1$	3 (3)	4 (4)	3 (3)	3 (3)
	NWHFC$_2$	3 (3)	4 (4)	3 (3)	3 (3)
	NWHFC$_3$	3 (3)	4 (4)	3 (3)	3 (3)
25 dB	NWEGA	**3**	**5**	**10**	**12**
	NWRMT	3	5	10	12
	HySime	3	5	8	9
	NWHFC$_1$	3 (3)	4 (4)	5 (5)	5 (5)
	NWHFC$_2$	3 (3)	4 (4)	5 (5)	5 (5)
	NWHFC$_3$	3 (3)	4 (4)	5 (5)	4 (4)
35 dB	NWEGA	**3**	**5**	**10**	**15**
	NWRMT	3	5	10	15
	HySime	3	5	10	13
	NWHFC$_1$	3 (3)	4 (4)	7 (7)	7 (7)
	NWHFC$_2$	3 (3)	4 (4)	7 (7)	6 (6)
	NWHFC$_3$	3 (3)	4 (4)	6 (6)	6 (6)
50 dB	NWEGA	**3**	**5**	**10**	**15**
	NWRMT	3	5	10	15
	HySime	3	5	10	14
	NWHFC$_1$	3 (3)	4 (4)	7 (7)	9 (9)
	NWHFC$_2$	3 (3)	4 (4)	7 (7)	8 (9)
	NWHFC$_3$	3 (3)	4 (4)	7 (7)	8 (8)

TABLE III
MEDIAN OF THE ESTIMATED K FOR DATA CORRUPTED BY COLORED
NOISE (GAUSSIAN SHAPE) WITH 50 MONTE CARLO SIMULATIONS.
FOR NWHFC, WE SHOW BETWEEN BRACKETS THE RESULTS WHEN
USING THE GROUND-TRUTH NOISE COVARIANCE MATRIX

SNR	Method	K=3	K = 5	K = 10	K = 15
15 dB	NWEGA	**3**	**5**	6	6
	NWRMT	3	5	5	5
	HySime	3	4	5	5
	NWHFC$_1$	3 (3)	5 (5)	8 (7)	9 (9)
	NWHFC$_2$	3 (3)	5 (5)	8 (7)	8 (8)
	NWHFC$_3$	3 (3)	5 (4)	7 (7)	8 (8)
25 dB	NWEGA	**3**	**5**	9	10
	NWRMT	3	5	8	9
	HySime	3	5	8	8
	NWHFC$_1$	3 (3)	5 (5)	8 (7)	9 (10)
	NWHFC$_2$	3 (3)	5 (5)	8 (7)	9 (9)
	NWHFC$_3$	3 (3)	5 (4)	8 (7)	8 (9)
35 dB	NWEGA	**3**	**5**	**10**	14
	NWRMT	3	5	10	13
	HySime	3	5	10	13
	NWHFC$_1$	3 (3)	5 (5)	9 (7)	11 (9)
	NWHFC$_2$	3 (3)	5 (4)	8 (7)	10 (8)
	NWHFC$_3$	3 (3)	5 (4)	8 (7)	9 (8)
50 dB	NWEGA	**3**	**5**	**10**	**15**
	NWRMT	3	5	10	15
	HySime	3	5	10	14
	NWHFC$_1$	7 (3)	9 (5)	14 (7)	18 (9)
	NWHFC$_2$	7 (3)	9 (5)	12 (7)	16 (9)
	NWHFC$_3$	6 (3)	7 (5)	11 (7)	15 (9)

V. SIMULATION RESULTS ON REAL DATA

A. Comparison With State-of-the-Art Algorithms

This section compares the NWEGA performance to that of the state-of-the-art algorithms by considering four real hyper-

spectral images. The performance of EGA is also presented to show the importance of the noise-whitening step. The first image (denoted by Madona) was acquired in 2010 by the Hyspex hyperspectral scanner over Villelongue, France (00 03' W and 4257' N). The data set contains $L = 160$ spectral bands recorded from the visible to near infrared (400–1000 nm) with a spatial resolution of 0.5 m [37]. The considered subset contains 702×1401 pixels and is mainly composed of forested areas [14], [30] as shown in RGB colors in Fig. 3(a). According to Sheeren *et al.* [37], the ground truth of this image contains 12 tree species that are as follows: ash tree, oak tree, hazel tree, locust tree, chestnut tree, lime tree, maple tree, beech tree, birch tree, willow tree, walnut tree, and fern. Consequently, the number of endmembers is expected to be at least equal to 12. Table IV (first column) shows the experimental results. The NWEGA estimated $K = 12$ endmembers, which is in agreement with the ground-truth information. The NWRMT, HFC, and NWHFC provided a larger estimate, while Hysime underestimated the number of endmembers. Note that the results obtained with HFC and NWHFC were expected since they estimate not only the endmember sources but also the interferences [2], [35].

The second image (denoted by Cuprite) was acquired by the Airborne Visible/Infrared Imaging Spectrometer (AVIRIS) over the Cuprite mining site, Nevada, in 1997. This image contains 182 spectral bands with a spectral resolution of 10 nm acquired in the 0.4–2.5-μm region (the water absorption bands 1–5, 105–115, 150–170, and 220–224 were removed) and a spatial resolution of 20 m [20], [38]. The considered image subset contains 351×351 pixels and is shown in RGB colors in Fig. 3(b). This image has been widely studied, and ground-truth information is available. According to USGS,[7] this image contains at least 18 minerals [39]. The considered algorithms were applied to this image, leading to the results in Table IV (second column). Except EGA, the algorithms estimated the number of endmembers to be larger than 18. NWEGA provided a more realistic value than NWRMT, which suffers from the spectral correlation when considering a multiple regression noise estimation algorithm [20]. However, the results obtained with Hysime, HFC, and NWHFC were in better agreement with the ground truth (closer to 18 endmembers).

The third image (denoted by Indian Pines) was also acquired by the AVIRIS sensor, in June 1992 over an agricultural area of the northwestern Indiana[8] (Indian Pines). The considered data set contains 145×145 pixels, 185 spectral bands with the same spectral resolution and spectral range as the Cuprite image (the water absorption bands 1–3, 103–113, 148–166, and 221–224 were removed), and a spatial resolution of 17 m [6]. As shown in Fig. 3(c), the observed image is a mixture of agriculture and forestry. According to the ground-truth information [6], [35], this image contains at least 16 endmembers that are as follows: alfalfa, corn-notill, corn-mintill, corn, grass-pasture, grass-trees, grass-pasture-mowed, hay-windrowed, oats, soybean-notill, soybean-mintill,
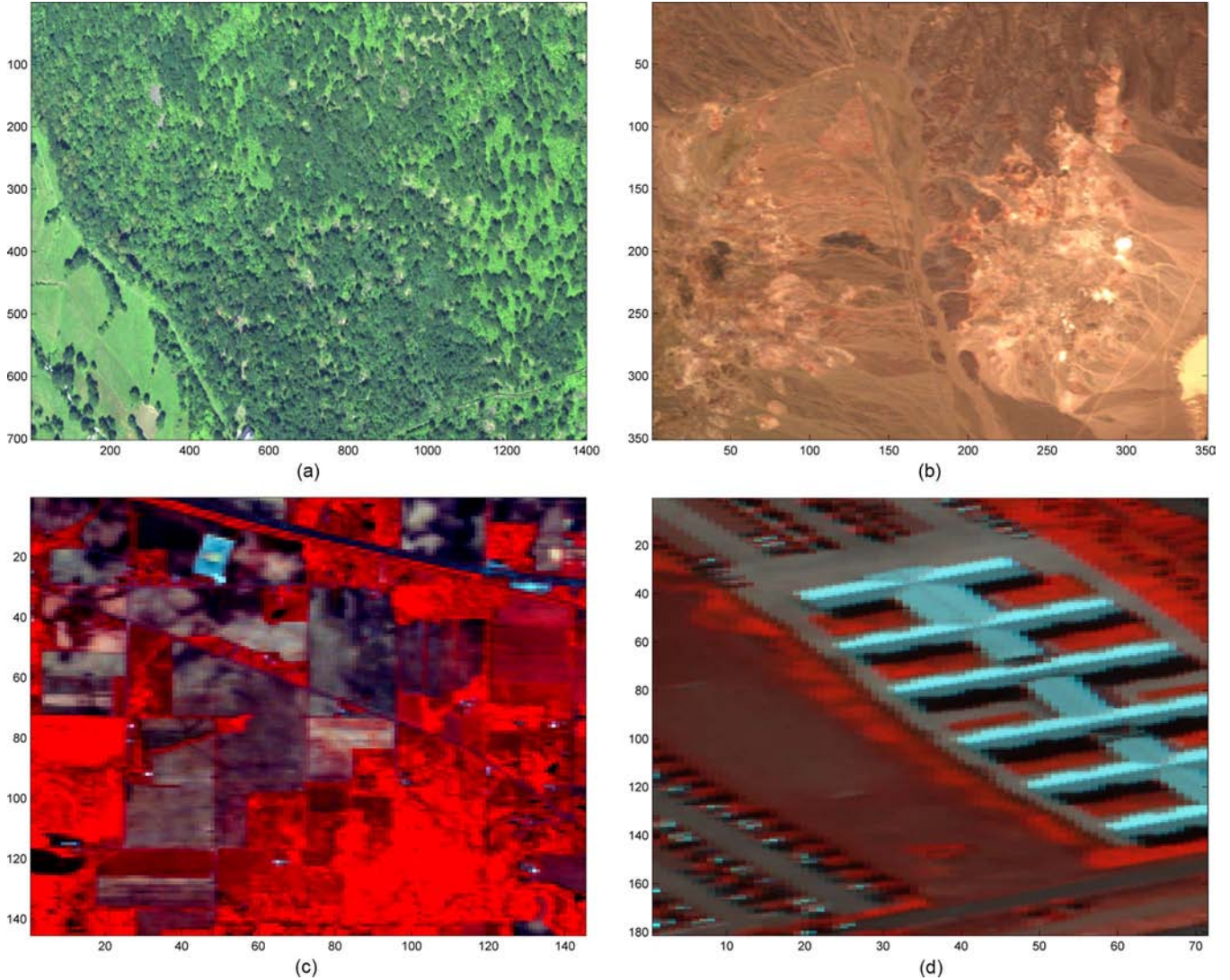
Fig. 3. Real images. (a) Hyspex Madonna image, (b) AVIRIS Cuprite scene, (c) AVIRIS Indian Pines, and (d) ROSIS Pavia University.

Method	Madonna	Cuprite	Indian Pines	Pavia university
Ground-truth	≥ 12	≥ 18	≥ 16	≥ 9
EGA	8	6	5	6
NWEGA	12	26	18	11
NWRMT	17	31	18	75
HySime	9	20	14	57
HFC_1	42	22	26	4
HFC_2	34	21	23	3
HFC_3	31	19	22	3
$NWHFC_1$	16	22	18	7
$NWHFC_2$	14	21	18	6
$NWHFC_3$	14	18	18	6

soybean-clean, wheat, woods, buildings-grass-trees-drives, and stone-steel-towers. Therefore, the estimated number should be greater than 16. Table IV (third column) reports the experimental results. Except Hysime that underestimated the number of endmembers and HFC that overestimated it, all algorithms detected 18 components in the Indian Pines image.

The fourth image (denoted by Pavia University) was acquired by the Reflective Optics System Imaging Spectrometer (ROSIS) sensor during a flight campaign over Pavia University, Italy.[9] This image contains 103 spectral bands with a spectral resolution of 4 nm acquired in the 0.4–0.9-μm region (the water absorption bands were removed) and a spatial resolution of 1.3 m. Fig. 3(d) shows the considered image of size 181 × 71 pixels. The ground truth of this image contains at least 9 endmembers consisting of asphalt, meadows, gravel, trees, painted metal sheets, bare soil, bitumen, self-blocking bricks, and shadows. As shown in Table IV (fourth column), both NWRMT and Hysime provide bad estimates, while HFC and NWHFC underestimate the number of endmembers. NWEGA estimates 11 endmembers, which is in better agreement with the ground truth (closer to nine endmembers).

The experimental results provided in this section illustrated the accuracy of the NWEGA when applied to real data, acquired by different sensors (AVIRIS, Hyspex, and ROSIS) and containing different physical elements (trees, grass, and minerals).

[9] Available: http://www.ehu.eus/ccwintco/index.php?title=Hyperspectral _Remote_Sensing_Scenes
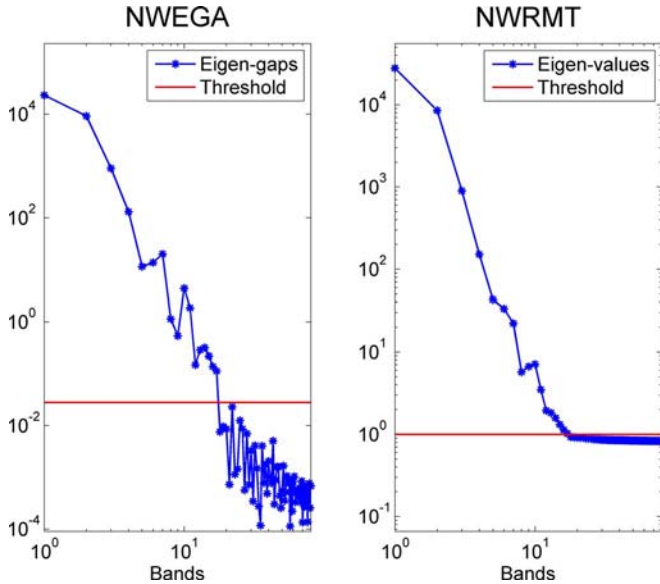
Fig. 4. Eigengap and eigenvalue (with whitening) repartitions for the Indian Pines image.
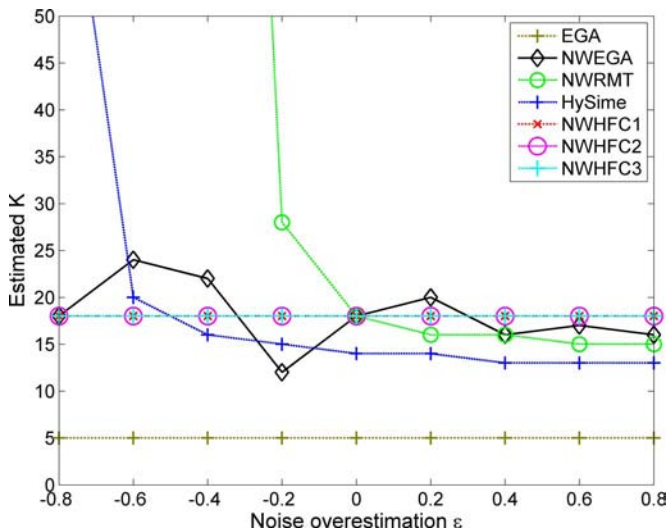

Fig. 5. Robustness of the algorithms w.r.t. the accuracy of the noise estimation for the Indian Pines image (ground truth ≥ 18).

B. Robustness to Noise and Image Size

This section analyzes the behavior of the NWEGA when considering the Indian Pines image. Fig. 4 shows the eigengaps and eigenvalues associated with the Indian Pines image. This figure highlights the higher level of separation between the signal and the noise obtained with the eigengaps when compared to the eigenvalues. To study the robustness of NWEGA w.r.t. additive noise, we corrupted the estimated noise covariance as in Section IV-A and considered the corrupted variances in the different algorithms. Fig. 5 shows the estimated numbers of endmembers for different values of ϵ. Similarly to the synthetic data, the NWRMT deviates first followed by the Hysime algorithm, while the proposed NWEGA and the different NWHFC are more robust to the presence of additive noise. Note that EGA provides poor results since it considers $\sigma^2 = 1$, which

TABLE V
ESTIMATED K W.R.T. THE IMAGE SIZE N FOR THE INDIAN PINES IMAGE

Method	$N = 16^2$	$N = 30^2$	$N = 60^2$	$N = 100^2$
Ground-truth	2	4	7	12
EGA	3	3	4	4
NWEGA	13	10	10	13
NWRMT	51	10	14	16
HySime	41	11	12	14
NWHFC$_1$	5	9	14	16
NWHFC$_2$	5	6	14	15
NWHFC$_3$	4	6	11	15

is too far from the estimated noise variances for the Indian Pines image. The last experiment studies the behavior w.r.t. the image size as shown in Table V. EGA provides a quite stable estimated number of endmembers that is much less than the ground truth for large image sizes. All other algorithms tend to overestimate the number of endmembers. The NWEGA provides quite competitive results when compared to the other methods. To conclude this section, the experiments conducted with the Indian Pines image tend to show that the proposed NWEGA algorithm is quite robust to the presence of additive noise and provides interesting results for different image sizes when compared to other state-of-the-art algorithms.

VI. CONCLUSION

This paper proposed a fully automatic algorithm for determining the number of endmembers in hyperspectral images. This algorithm consisted of two steps that are noise estimation and determination of the endmember number. Noise estimation was achieved by a multiple regression estimation method even if other algorithms could be investigated. The second step was performed by thresholding the difference between successive eigenvalues of the sample covariance matrix. The resulting algorithm is nonparametric (it does not require any user-determined parameter) and efficient in the presence of i.i.d. and colored noise. Synthetic experiments showed a robust behavior of NWEGA w.r.t. noise estimation errors, noise correlations, and noise levels. It also showed good performance when considering different image sizes. The obtained results on real images confirmed the accuracy of the proposed algorithm that showed comparable or better results than some state-of-the-art algorithms. Future work includes the study of robust estimation for the pixel covariance matrix. Considering the recent method proposed in [27], [40], and [41] for source detection is also an interesting issue which would deserve to be investigated.

APPENDIX
HYPOTHESES

This appendix describes some assumptions required for the RMT to be applied. Note that the Gaussianity of the additive noise is not necessary and only a finite eighth-order moment is required on the entries [24]. Moreover, the assumptions described in Section II-C are more specific than the classical assumptions used in the RMT literature as follows [42].

1) $\mathbf{\Lambda}$ has uniformly bounded spectral norm $\forall L \in \mathbb{N}^*$, i.e., $\forall i \in [1, L], \lambda_i < \infty$.

2) Let $\boldsymbol{E} \in \mathbb{R}^{L \times N}$ have i.i.d. entries e_{ij} with zero mean and unit variance and be absolutely continuous with $E[|e_{ij}|^8] < 1$.

3) Let $\boldsymbol{E} \in \mathbb{R}^{L \times N}$ be defined as in (2) then, its distribution is invariant by left multiplication by a deterministic unitary matrix. Moreover, the eigenvalue empirical PDF of $(1/N)\boldsymbol{E}\boldsymbol{E}^{\top}$ a.s. converges to the Marcenko–Pastur distribution with support $[(1 - \sqrt{c})^2, (1 + \sqrt{c})^2]$.

4) The maximum (respectively minimum) eigenvalue of $(1/N)\boldsymbol{E}\boldsymbol{E}^{\top}$ a.s. tends to $(1 + \sqrt{c})^2$ (respectively to $(1 - \sqrt{c})^2$).

5) The eigenvalues γ_r, $r = 1, \ldots, R$, satisfy the separation condition.

REFERENCES

[1] N. Keshava and J. F. Mustard, "Spectral unmixing," *IEEE Signal Process. Mag.*, vol. 19, no. 1, pp. 44–57, Jan. 2002.

[2] J. Bioucas-Dias *et al.*, "Hyperspectral unmixing overview: Geometrical, statistical, and sparse regression-based approaches," *IEEE J. Sel. Topics Appl. Earth Observ. Remote Sens.*, vol. 5, no. 2, pp. 354–379, Apr. 2012.

[3] N. Dobigeon *et al.*, "Nonlinear unmixing of hyperspectral images: Models and algorithms," *IEEE Signal Process. Mag.*, vol. 31, no. 1, pp. 82–94, Jan. 2014.

[4] A. Halimi, Y. Altmann, N. Dobigeon, and J.-Y. Tourneret, "Nonlinear unmixing of hyperspectral images using a generalized bilinear model," *IEEE Trans. Geosci. Remote Sens.*, vol. 49, no. 11, pp. 4153–4162, Nov. 2011.

[5] Y. Altmann, A. Halimi, N. Dobigeon, and J.-Y. Tourneret, "Supervised nonlinear spectral unmixing using a postnonlinear mixing model for hyperspectral imagery," *IEEE Trans. Image Process.*, vol. 21, no. 6, pp. 3017–3025, Jun. 2012.

[6] J. M. Bioucas-Dias and J. M. P. Nascimento, "Hyperspectral subspace identification," *IEEE Trans. Geosci. Remote Sens.*, vol. 46, no. 8, pp. 2435–2445, Aug. 2008.

[7] C. Chang and Q. Du, "Estimation of number of spectrally distinct signal sources in hyperspectral imagery," *IEEE Trans. Geosci. Remote Sens.*, vol. 42, no. 3, pp. 608–619, Mar. 2004.

[8] J. M. Nascimento and J. M. Bioucas-Dias, "Vertex component analysis: A fast algorithm to unmix hyperspectral data," *IEEE Trans. Geosci. Remote Sens.*, vol. 43, no. 4, pp. 898–910, Apr. 2005.

[9] N. Dobigeon, S. Moussaoui, M. Coulon, J.-Y. Tourneret, and A. O. Hero, "Joint Bayesian endmember extraction and linear unmixing for hyperspectral imagery," *IEEE Trans. Signal Process.*, vol. 57, no. 11, pp. 4355–4368, Nov. 2009.

[10] D. C. Heinz and C.-I. Chang, "Fully constrained least-squares linear spectral mixture analysis method for material quantification in hyperspectral imagery," *IEEE Trans. Geosci. Remote Sens.*, vol. 29, no. 3, pp. 529–545, Mar. 2001.

[11] J. Chen, C. Richard, and P. Honeine, "Nonlinear estimation of material abundances in hyperspectral images with ℓ_1-norm spatial regularization," *IEEE Trans. Geosci. Remote Sens.*, vol. 52, no. 5, pp. 2654–2665, May 2014.

[12] N. H. Nguyen, J. Chen, C. Richard, P. Honeine, and C. Theys, "Supervised nonlinear unmixing of hyperspectral images using a pre-image methods," *EAS Publications Series*, vol. 59, pp. 417–437, Jan. 2013.

[13] R. Ammanouil, A. Ferrari, C. Richard, and D. Mary, "Blind and fully constrained unmixing of hyperspectral images," *IEEE Trans. Image Process.*, vol. 23, no. 12, pp. 5510–5518, Dec. 2014.

[14] A. Halimi, N. Dobigeon, and J.-Y. Tourneret, "Technical report associated with the paper 'Unsupervised unmixing of hyperspectral images accounting for endmember variability'," Univ. Toulouse, Toulouse, France, Tech. Rep., May 2014. [Online]. Available: https://sites.google.com/site/abderrahimhalimi/publications.

[15] P. Honeine and C. Richard, "Geometric unmixing of large hyperspectral images: A barycentric coordinate approach," *IEEE Trans. Geosci. Remote Sens.*, vol. 50, no. 6, pp. 2185–2195, Jun. 2012.

[16] H. Akaike, "A new look at the statistical model identification," *IEEE Trans. Autom. Control*, vol. 19, no. 6, pp. 716–723, Dec. 1974.

[17] G. Schwarz, "Estimating the dimension of a model," *Ann. Statist.*, vol. 6, no. 2, pp. 461–464, 1978.

[18] J. Rissanen, "Modeling by shortest data description," *Automatica*, vol. 14, pp. 465–471, 1978.

[19] B. Luo, J. Chanussot, S. Doute, and L. Zhang, "Empirical automatic estimation of the number of endmembers in hyperspectral images," *IEEE Geosci. Remote Sens. Lett.*, vol. 10, no. 1, pp. 24–28, Jan. 2013.

[20] K. Cawse-Nicholson, A. B. Damelin, A. Robin, and M. Sears, "Determining the intrinsic dimension of a hyperspectral image using random matrix theory," *IEEE Trans. Image Process.*, vol. 22, no. 4, pp. 1301–1310, Apr. 2013.

[21] K. Cawse-Nicholson, A. Robin, and M. Sears, "The effect of noise whitening on methods for determining the intrinsic dimension of a hyperspectral image," in *Proc. IEEE GRSS WHISPERS*, Lisbon, Portugal, Jun. 2011, pp. 1–4.

[22] K. Cawse-Nicholson, A. Robin, and M. Sears, "The effect of spectrally correlated noise on noise estimation methods for hyperspectral images," in *Proc. IEEE GRSS WHISPERS*, Shanghai, China, Jun. 2012, pp. 1–4.

[23] I. M. Johnstone, "On the distribution of the largest eigenvalue in principal component analysis," *Ann. Statist.*, vol. 29, pp. 295–327, 2001.

[24] D. Passemier and J. F. Yao, "On determining the number of spikes in a high-dimensional spiked population model," *Random Matrices, Theory Appl.*, vol. 1, p. 19, 2012.

[25] S. Kritchman and B. Nadler, "Non-parametric detection of the number of signals: Hypothesis testing and random matrix theory," *IEEE Trans. Signal Process.*, vol. 57, no. 10, pp. 3930–3941, Oct. 2009.

[26] J. Baik and J. W. Silverstein, "Eigenvalues of large sample covariance matrices of spiked population models," *J. Multivariate Anal.*, vol. 97, no. 6, pp. 1382–1408, Jul. 2006.

[27] D. Passemier, "Inférence statistique dans un modèle à variance isolée de grande dimension," Ph.D. dissertation, Dept. Statistiques, Univ. Rennes 1, Rennes, France, 2012.

[28] R. Couillet and W. Hachem, "Fluctuations of spiked random matrix models and failure diagnosis in sensor networks," *IEEE Trans. Inf. Theory*, vol. 59, no. 1, pp. 509–525, Jan. 2013.

[29] A. Onatski, "Testing hypotheses about the number of factors in large factors models," *Econometrica*, vol. 77, no. 5, pp. 1447–1479, Sep. 2009.

[30] Y. Altmann, N. Dobigeon, S. McLaughlin, and J.-Y. Tourneret, "Unsupervised post-nonlinear unmixing of hyperspectral images using a Hamiltonian Monte Carlo algorithm," *IEEE Trans. Image Process.*, vol. 23, no. 6, pp. 2663–2675, Jun. 2014.

[31] A. Green, M. Berman, P. Switzer, and M. Craig, "A transformation for ordering multispectral data in terms of image quality with implications for noise removal," *IEEE Trans. Geosci. Remote Sens.*, vol. GE-26, no. 1, pp. 65–74, Jan. 1988.

[32] P. Meer, J. Jolion, and A. Rosenfeld, "A fast parallel algorithm for blind estimation of noise variance," *IEEE Trans. Pattern Anal. Mach. Intell.*, vol. 12, no. 2, pp. 216–223, Feb. 1990.

[33] R. E. Roger and J. F. Arnold, "Reliably estimating the noise in AVIRIS hyperspectral images," *Int. J. Remote Sens.*, vol. 17, no. 10, pp. 1951–1962, 1996.

[34] K. Cawse-Nicholson, A. Robin, and M. Sears, "The effect of correlation on determining the intrinsic dimension of a hyperspectral image," *IEEE J. Sel. Topics Appl. Earth Observ. Remote Sens.*, vol. 6, no. 2, pp. 482–487, Apr. 2013.

[35] C. Andreou and V. Karathanassi, "Estimation of the number of endmembers using robust outlier detection method," *IEEE J. Sel. Topics Appl. Earth Observ. Remote Sens.*, vol. 7, no. 1, pp. 247–256, Jan. 2014.

[36] A. Halimi, P. Honeine, M. Kharouf, C. Richard, and J.-Y. Tourneret, "Estimating the intrinsic dimension of hyperspectral images using an eigen-gap approach," 2015, unpublished paper. [Online]. Available: http://arxiv.org/abs/1501.05552.

[37] D. Sheeren *et al.*, "Mapping ash tree colonization in an agricultural mountain landscape: Investigating the potential of hyperspectral imagery," in *Proc. IEEE IGARSS*, Jul. 2011, pp. 3672–3675.

[38] F. A. Kruze, "Comparison of AVIRIS and Hyperion for hyperspectral mineral mapping," in *Proc. 11th JPL Airborne Geosci. Workshop*, 2002, pp. 1–11.

[39] G. Swayze, R. Clark, S. Sutley, and A. Gallagher, "Ground-truthing AVIRIS mineral mapping at Cuprite, Nevada," in *Proc. Summaries 3rd Annu. JPL Airborne Geosci. Workshop*, 1992, vol. 1, pp. 47–49.

[40] J. Vinogradova, R. Couillet, and W. Hachem, "Statistical inference in large antenna arrays under unknown noise pattern," *IEEE Trans. Signal Process.*, vol. 61, no. 22, pp. 5633–5645, Nov. 2013.

[41] J. Vinogradova, R. Couillet, and W. Hachem, "A new method for source detection, power estimation, and localization in large sensor networks under noise with unknown statistics," in *Proc. IEEE ICASSP*, May 2013, pp. 3943–3946.

[42] A. Combernoux, F. Pascal, G. Ginolhac, and M. Lesturgie, "Convergence of structured quadratic forms with application to theoretical performances of adaptive filters in low rank Gaussian context," 2015, unpublished paper. [Online]. Available: http://arxiv.org/abs/1503.05480.

Abderrahim Halimi (S'11–M'14) received the Eng. degree in electronics from the National Polytechnic School of Algiers, Algiers, Algeria, in 2009 and the M.Sc. and Ph.D. degrees in signal processing from the Institut National Polytechnique de Toulouse, Toulouse, France, in 2010 and 2013, respectively.

From October 2013 to September 2014, he has been a Postdoctoral Research Associate with the Institut de Recherche en Informatique de Toulouse, University of Toulouse, Toulouse. He is currently a Postdoctoral Research Associate with the University of Technology of Troyes, Troyes, France. His research activities focus on statistical signal and image processing, with a particular interest in Bayesian inverse problems with applications to hyperspectral imaging and altimetry.

Paul Honeine (M'07) was born in Beirut, Lebanon, on October 2, 1977. He received the Dipl.Ing. degree in mechanical engineering and the M.Sc. degree in industrial control from the Lebanese University, Beirut, in 2002 and 2003, respectively, and the Ph.D. degree in systems optimization and security from the University of Technology of Troyes, Troyes, France, in 2007.

He was a Postdoctoral Research Associate with the Systems Modeling and Dependability Laboratory from 2007 to 2008. From September 2008 to August 2015, he was an Assistant Professor at the University of Technology of Troyes, Troyes. Since September 2015, he has been a Full Professor at the Laboratoire d'Informatique, du Traitement de l'Information et des Systemes (LITIS) of the University of Rouen, Rouen, France. His research interests include nonstationary signal analysis and classification, nonlinear and statistical signal processing, sparse representations, and machine learning. Of particular interest are applications to (wireless) sensor networks, biomedical signal and image processing, hyperspectral imagery, and nonlinear adaptive system identification.

Dr. Honeine is the coauthor (with C. Richard) of the 2009 Best Paper Award at the IEEE Workshop on Machine Learning for Signal Processing.

Malika Kharouf received the Ph.D. degree in applied mathematics from Télécom ParisTech, Paris, France, in 2010.

From September 2009 to August 2011, she was a temporary Lecturer and Research Assistant at University Paris 10. After this, she spent one year as a Postdoctoral Researcher in the Gaspard-Monge laboratory at University Marne La Vallée, from October 2011 to September 2012. Then, she was a Postdoctoral Researcher in the School of Physical and Mathematical Sciences, Nanyang Technological University of Singapore, until August 2013. She is currently an Associate Professor at the University of Technology of Troyes, Troyes, France. Her research interests include high-dimensional statistics, probability at large, and random matrix theory.

Cédric Richard (S'98–M'01–SM'07) received the Dipl.Ing., M.S., and Ph.D. degrees in electrical and computer engineering from the Compiègne University of Technology, Compiègne, France, in 1994 and 1998, respectively.

He was an Associate Professor at the University of Technology of Troyes, Troyes, from 1999 to 2003 and a Full Professor from 2003 to 2009. Since 2009, he has been a Full Professor at the University of Nice Sophia Antipolis, Nice, France. He has been a junior member of the Institut Universitaire de France since 2010. His current research interests include statistical signal processing and machine learning. He is the author of over 230 papers.

Dr. Richard was the General Cochair of the IEEE SSP Workshop that was held in Nice, in 2011. He was the Technical Cochair of EUSIPCO 2015 that was held in Nice, and of the IEEE CAMSAP Workshop 2015 that was held in Cancun, Mexico. He serves as a Senior Area Editor of the IEEE TRANSACTIONS ON SIGNAL PROCESSING and as an Associate Editor of the IEEE TRANSACTIONS ON SIGNAL AND INFORMATION PROCESSING OVER NETWORKS since 2015. He is also an Associate Editor of the journal *Signal Processing* since 2009. He is a member of the Machine Learning for Signal Processing Technical Committee and served as a member of the Signal Processing Theory and Methods Technical Committee in 2009–2014.

Jean-Yves Tourneret (SM'08) received the ingénieur degree in electrical engineering from the Ecole Nationale Supérieure d'Electronique, d'Electrotechnique, d'Informatique, d'Hydraulique et des Télécommunications (ENSEEIHT), Toulouse, France, in 1989 and the Ph.D. degree from the National Polytechnic Institute of Toulouse, Toulouse, in 1992.

He is currently a Professor in the University of Toulouse (ENSEEIHT) and a member of the IRIT laboratory (UMR 5505 of the CNRS). His research activities are centered around statistical signal and image processing with a particular interest to Bayesian and Markov chain Monte Carlo methods.

Dr. Tourneret has been involved in the organization of several conferences, including the European conference on signal processing EUSIPCO'02 (Program Chair), the international conference ICASSP'06 (plenaries), the statistical signal processing workshop SSP'12 (international liaisons), the International Workshop on Computational Advances in Multi-Sensor Adaptive Processing CAMSAP 2013 (local arrangements), the statistical signal processing workshop SSP'2014 (special sessions), and the workshop on machine learning for signal processing MLSP'2014 (special sessions). He has been the General Chair of the CIMI workshop on optimization and statistics in image processing held in Toulouse in 2013 (with F. Malgouyres and D. Kouamé) and of the International Workshop on Computational Advances in Multi-Sensor Adaptive Processing CAMSAP 2015 (with P. Djuric). He has been a member of different technical committees, including the Signal Processing Theory and Methods committee of the IEEE Signal Processing Society (2001–2007, 2010–present). He has been serving as an Associate Editor for the IEEE TRANSACTIONS ON SIGNAL PROCESSING (2008–2011, 2015–PRESENT) and for the *EURASIP Journal on Signal Processing* (since July 2013).